

Vibrationally Inelastic Low-Energy CO⁺ - Ar Collisions*

Frederick Petty and T. F. Moran

School of Chemistry, Georgia Institute of Technology, Atlanta, Georgia 30332

(Received 16 April 1971)

Relative differential cross sections for inelastic scattering of CO⁺ by Ar have been examined with a high-resolution ion-beam apparatus in which a CO⁺ beam interacts with a neutral-Ar beam and the energy, mass, and angular distribution of scattered ions are measured. Maxima in the inelastic energy-loss spectra occur at energies corresponding to CO⁺ spectroscopic vibrational spacings. The probabilities of multiquantum vibrational transitions are found to increase with both reactant-ion kinetic energy and scattering angle. Cross sections for vibrational excitation at small scattering angles are adequately described by a semiclassical oriented-nonlinear-encounter model in which an impact-parameter treatment is used to estimate collisional energy transfer for a forced oscillator, and time-dependent wave functions employed to evaluate vibrational transition probabilities. The energy width of the inelastic peaks indicated that simultaneous vibrational-rotational excitations occur. Weakly inelastic processes are observed below the threshold for vibrational energy loss, corresponding to rotational excitation with the relative importance of rotational transitions increasing with decreasing energy and scattering angle.

INTRODUCTION

Energy conversion between translational and molecular internal degrees of freedom in bimolecular collisions has been the subject of many theoretical and experimental investigations. Theoretical calculations¹⁻¹⁴ on simple systems such as the archetypal encounter $A + BC$ have ranged from exact quantum mechanical calculations for He-H₂ interactions¹⁵ to exact classical treatments.^{16,17} Between these extremes are semiclassical approaches⁸⁻¹⁰ in which collisions are described in terms of a quantum oscillator perturbed by a force derived from the intermolecular interaction potential. Much of the present experimental knowledge on this subject has been obtained from spectroscopic relaxation methods¹⁸⁻²⁰ by which it is difficult to extract angular and velocity dependences of inelastic events. Recent experiments²¹⁻²⁷ have applied beam techniques to the problem of obtaining the elusive but important differential inelastic cross sections. In these investigations a velocity-selected ion beam interacted with neutral target molecules and the energy spectra of inelastically scattered ions was determined using either time-of-flight techniques^{21,22} or electrostatic energy analysis.²³⁻²⁶ From a kinematic analysis²¹ of the inelastic spectra vibrational transition probabilities were obtained. Probabilities of multiquantum vibrational transitions were found to increase with both incident-ion translational energy and scattering angle.^{24,25} The purpose of the present study is to investigate collisional excitation of diatomic molecule ions with an ion-impact spectrometer capable of fully resolving discrete vibrational transitions in the inelastic energy-loss spectrum. Our objective is to examine the applicability of theoretical

models to simple systems and obtain insight into the relevant energy-conversion processes.

APPARATUS

The ion-impact spectrometer (Fig. 1) used to measure the inelastic energy-loss spectra consists of two 127° electrostatic sectors, an ion source, a collision chamber, focusing and angle-defining slits, a Paul-Steinwedel mass filter,²⁸ a channel electron multiplier,²⁹ and associated electronics.

Ions are generated in a variable energy gas-phase electron-impact source and extracted from the source by a weak drawout potential, accelerated through a split-plate focusing slit, then decelerated before entry into the primary-ion energy-controlling sector. Cylindrical geometry for this sector is defined by fine-mesh wire screens of high transmittance to reduce space charge caused by out-of-focus ions and provide nonsputtering surfaces. The curved plates shown in Fig. 1 outside the wire screen of this sector were maintained at a slightly negative potential in order to attract ions that passed through the screens and to prevent space charge buildup in the sector region. The sector design is similar to those used in electron scattering experiments.³⁰ The kinetic energy calibration of the first sector was carried out in separate experiments using a standard³¹ retarding-analysis arrangement. Prescriptions³¹ for determining focus conditions for ions passing through such a sector are found to hold here. Ion transmission by the sector is slightly improved with a positive voltage on z -axis focus plates with negligible perturbation of reactant-ion kinetic energy distribution. The second sector shown in Fig. 1 was then inserted in the analyzing system and calibrated with the aid of the primary-ion sector. Since it is possible

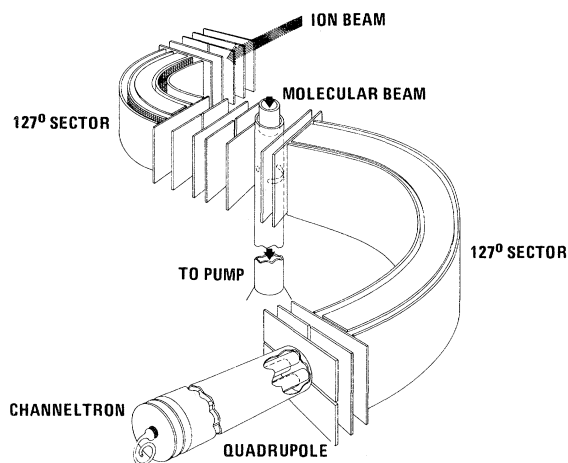


FIG. 1. Schematic diagram of ion-impact spectrometer used to measure energy-loss spectra of CO^+ inelastically scattered from Ar. Ions are produced by gas-phase variable-energy electron impact ionization and are energy selected prior to ion-molecule collision. Scattered-ion energy and mass analysis are accomplished with the electrostatic-sector mass-filter combination. The entire detection train is rotatable about the collision chamber to provide scattering-angle analysis.

for ions exiting a 127° electrostatic sector to spatially diverge past the focal point, we found it necessary to collimate geometrically the primary-ion beam with a 0.008-in.-wide slit system prior to entrance into the collision region in order to insure parallel ion-beam rays for the ion-molecule interaction. Scattered product ions emerging from the interaction region pass through an analyzing-slit system with a 0.8° angular resolution which is used to define the scattering volume. The kinetic energy spread of the primary-ion beam was determined to be typically 0.04 eV full width at half-maximum (FWHM). During measurements of inelastic energy-loss spectra, the kinetic energy and angular distributions of both the primary and elastically scattered ion beams were frequently checked to insure that the integrity of the kinetic energy distribution of the primary-ion beam was maintained and that the system was functioning properly as a complete unit. Voltages to all ion optics are stable to less than 1 mV/h. No evidence for buildup of contamination on potential-defining surfaces in the path of the primary or scattered-ion beam was observed. Slight long-term variations of the primary-ion beam intensity were noted after approximately 80 h of running the electron-impact ion source. These slight long-term variations were correlated with changes in electron beam current and were corrected by abrasive and solvent cleaning of the ion-source areas in close proximity to the thoriated iridium filament. Filament emission was regulated by an electron-trap current feedback

loop similar to that used in commercial mass spectrometers.

The primary-ion source was designed to be gas tight with molecular flow out of the source region through the ion-beam slit. Separate gas handling systems were used for the source and ion-molecule collision regions and consisted of regulated high-pressure gas supplies with fine needle valves controlling pressure to 10-liter ballast tanks with gas flow from these tanks into the ion-impact spectrometer through fixed aperture leaks. These extra ballasts have provided extremely constant gas densities in the respective regions of the apparatus. Constant molecular concentrations were necessary to insure stability of the primary and scattered-ion beams. Neutral target atoms enter the collision chamber through a multichannel fused-glass capillary array³² which aims a primarily mono-directional beam of target atoms into a well defined ion-molecule interaction region. The neutral target molecules then flow directly into a high-speed diffusion pump. Scattered product ions from the ion-neutral-molecular interactions pass into the detection system consisting of angle-defining slits, the 127° analyzing sector, and quadrupole mass filter equipped with a channel electron multiplier. Pulses from the channeltron output are amplified, shaped, and digitally recorded using an ORTEC counting system. The scattered-ion detection system may be rotated about the collision chamber to 90° with respect to the incident-ion beam. This entire apparatus is mounted on an optical bench inside a 32-in.-diam stainless-steel high-vacuum chamber.

RESULTS AND DISCUSSION

Recent experiments have shown ion-beam techniques²¹⁻²⁶ to be a useful tool with which to examine energy transfer processes in intermolecular collisions. Products resulting from ion-molecule interactions may be elastically or inelastically scattered. The processes are distinguished by energy analysis in a high-resolution apparatus. Energy and momentum conservation laws provide the necessary relationship between momentum vectors of scattered products so that the energy of elastic and inelastic products can be computed and thus compared with experiment. For the interaction of an ion of mass M and initial kinetic energy E_0 with a stationary neutral target molecule of mass m , the momentum P of the scattered ions can be determined from

$$P = F \cos\Theta \pm (R^2 - F^2 \sin^2\Theta)^{1/2}. \quad (1)$$

Θ is the laboratory scattering angle, F is the momentum of the center of mass of the system, and R is the momentum of the scattered ion with respect to the center of mass. The following relations defining F and R are obtained from the mechanics of

collision:

$$\begin{aligned} F^2 &= 2M^3 E_0 / (M+m)^2, \quad E_s = mE_0 / (M+m), \\ R_e &= mF/M, \quad R_i = mF(1 - \Delta E/E_s)^{1/2}/M, \\ E &= p^2/2M, \end{aligned} \quad (2)$$

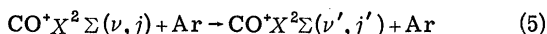
where ΔE is the spectroscopic energy loss. The subscripts e and i refer to elastic and inelastic scattering parameters, respectively. The difference between the energy of elastically and inelastically scattered ions at a particular angle Θ is given by

$$\begin{aligned} E_e - E_i &= \frac{m\Delta E}{M+m} \pm \frac{2ME_0 \cos\Theta}{(M+m)^2} \\ &\times \left\{ (m^2 - M^2 \sin^2\Theta)^{1/2} - \left[1 - \frac{(M+m)\Delta E}{ME_0} \right]^{1/2} \right. \\ &\times \left. \left[m^2 - \frac{M^2 \sin^2\Theta}{1 - [(M+m)\Delta E/mE_0]} \right]^{1/2} \right\} \end{aligned} \quad (3)$$

using the relationships in Eqs. (1) and (2). The inelasticity $E_e - E_i$ for interactions between mass identified reactants of a given energy at a particular lab angle can be computed from Eq. (3) using spectroscopic energy differences calculated from

$$\begin{aligned} \Delta E &= hc\omega_e(\nu' - \nu) - hc\omega_e\lambda_e \left[(\nu' + \frac{1}{2})^2 - (\nu + \frac{1}{2})^2 \right] \\ &+ (h^2/8\pi^2 I) [(j'+1) - j(j+1)]. \end{aligned} \quad (4)$$

ν and j are vibrational and rotational quantum numbers of the diatomic species, I is its moment of inertia, and primed quantum numbers are those of the final states. It is not necessary to include electronic excitation in the computation of ΔE for the inelastic



collisions examined in this paper, although such processes are evident in experiments³³⁻³⁵ carried out at much higher reactant-ion kinetic energies. 60-V electrons were used throughout these investigations to ionize the neutral CO molecules. The absolute energy of the ionizing electron beam was calculated by comparison of experimentally measured ionization potentials of various atoms and molecules with known spectroscopic ionization potentials. High-energy electron impact ionization of CO results in formation³⁶ of CO^+ ions in the ground $X^2\Sigma$ and also the $A^2\pi$ and $B^2\Sigma$ electronically excited states. Cross sections for 60-eV electron impact ionization of CO, forming ions in these different electronic states, have been determined³⁷ so that the initial electronic state distribution of our CO^+ reactant-ion beam has been estimated and the vibrational distribution in each of these states computed from vibrational transition probabilities using the respective Franck-Condon factors.^{38,39} The flight time for reactant CO^+ ions to pass from

the electron beam to the exit slit of the primary-ion sector is longer than 2×10^{-5} sec. Spontaneous $A \rightarrow X$ (Refs. 40-43) and $B \rightarrow X$ (Refs. 40 and 44) radiative transitions take place in 4.5×10^{-8} and 2.6×10^{-6} sec, respectively, with the result that the CO^+ reactant ion beam is in the ground $X^2\Sigma$ state prior to ion-neutral-molecule interaction in the collision region. The vibrational distribution of the $\text{CO}^+ X^2\Sigma$ ground electronic state has been computed from $\text{CO} X^1\Sigma \rightarrow \text{CO}^+(X, A, B)$ Franck-Condon factors weighted according to respective electron impact ionization cross sections and corresponding Franck-Condon factors for spontaneous $A \rightarrow X$ (Refs. 39 and 45) and $B \rightarrow X$ (Ref. 45) radiative transitions. The computed $\text{CO}^+ X^2\Sigma$ reactant-ion vibrational population is $\nu=0, 0.60; \nu=1, 0.12; \nu=2, 0.084; \nu=3, 0.061; \nu=4, 0.049; \nu=5, 0.035$, with a rapid decrease at higher vibrational levels. For all practical purposes, ΔE can be computed by considering all the $\text{CO}^+ X^2\Sigma$ reactant ions to be in the $\nu=0$ vibrational level although measured inelastic ion-molecule collisions with energy loss corresponding to $|\Delta\nu|=1$ can contain some contributions from inelastic $\Delta\nu=1-2$, etc., transitions. Inelastic scattering events involving a given change in vibrational quantum number from different initial vibrational levels will not be resolvable in the present experiments with the 0.04 eV FWHM primary-ion kinetic energy distribution. For example, the spectroscopic energy difference⁴⁶ between levels corresponding to a $\Delta\nu=4 \rightarrow 5$ vibrational transition is 0.256 eV, which is to be compared with the $\Delta\nu=0 \rightarrow 1$ transition, where ΔE is 0.271 eV. As will be shown in the figures presenting the experimental energy-loss spectra, this typical 0.051 eV spectroscopic energy spread that is possible for transitions involving different initial $\text{CO}^+ X^2\Sigma$ vibrational levels will be smaller than the width of the arrows denoting positions of various vibrational transitions as a function of $E_e - E_i$.

Scattered CO^+ product-ion distributions from $\text{CO}^+ X^2\Sigma + \text{Ar}$ interactions contain both elastic and inelastic contributions. The elastically scattered ion intensity increases as the scattering angle decreases, a result similar to that observed in other measurements^{47,48} and theoretical descriptions.⁴⁹⁻⁵¹ Energetic positions of elastic peaks as a function of the lab scattering angle are given by

$$\begin{aligned} E_e &= (F^2/M) \{ 2 \cos^2\Theta - 1 + m^2/M^2 \\ &+ [(2 \cos\Theta)/M](m^2 - M^2 \sin^2\Theta)^{1/2} \}. \end{aligned} \quad (6)$$

We have used elastically scattered product ions as a convenient point to reference the inelastic spectra since the elastic peak establishes the zero of energy for inelastic collisions measured at a given lab scattering angle. The 0.04 eV energy FWHM of the primary-ion beam is sufficiently

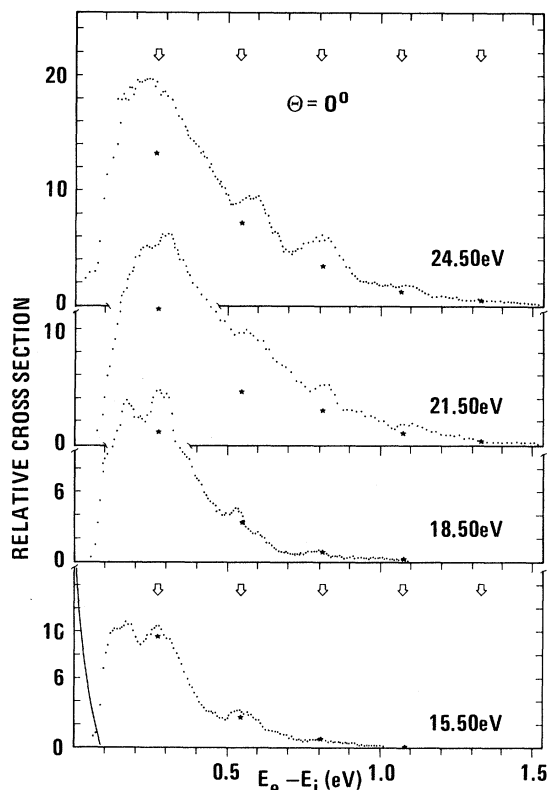


FIG. 2. Energy-loss spectra of CO^+ . Relative differential cross sections for inelastic CO^+ -Ar collisions vs inelasticity of collisions, $E_e - E_i$, at 0° lab scattering angle and several incident-ion energies (E_0). The dots are experimental data. Arrows indicate calculated energy loss corresponding to vibrational $\nu=0 \rightarrow 1, \dots, 5$ excitation by collision, and stars indicate cross sections for each vibrational transition theoretically predicted by an oriented nonlinear encounter model, with calculated probabilities averaged over all molecular orientations.

narrow to allow complete separation of elastic from inelastic interactions corresponding to a change in CO^+ vibrational quantum number $\Delta\nu=1$. Typical inelastic energy-loss spectra are given in Fig. 2 for collisions of 24.50–15.50 eV lab energy CO^+ reactant ions measured at nominal 0° lab angle. In this figure measured differential inelastic cross sections are presented as a function of collisional energy loss $E_e - E_i$. Arrows in this figure show predicted positions of $\nu=0 \rightarrow 1, \dots, 5$ vibrational transitions calculated using Eq. (3) with ΔE computed from tabulated $\text{CO}^+X^2\Sigma$ spectroscopic constants.^{46,52} Maxima in the inelastic energy-loss spectra are observed at energetic positions computed for vibrational excitations. Relative differential cross sections, $\bar{I}(\Theta)$, have been obtained from scattered-ion intensities by use of the equation

$$\bar{I}(\Theta) = i_s/i_0 g(\Theta)k, \quad (7)$$

in which i_s and i_0 are intensities of the scattered and incident beam, $g(\Theta)$ is the fraction of the scattering volume²⁵ subtended by the detector at the laboratory scattering angle Θ , and k includes a term to account for target-gas density and the energy dependence of analyzing-sector transmissivity. $g(\Theta)$ has been determined from the slit sizes and distances between slits placed before and after the collisions region. The primary-ion focal point at the end of the first sector is sharp but the ion beam spatially diverges from this point and thus it is necessary to place a beam-defining slit system after the first sector in front of the collision region. This reduces primary-ion intensity along with improving the angular spread of the primary-ion beam to less than 1° , a spread which is expected from geometrical consideration. At 0° lab scattering angle there is a slight tailing of the primary-ion beam to approximately 0.125 eV from the center of its kinetic energy distribution, which is shown as the solid curve in Fig. 2. We note that the primary-ion beam does not interfere with observation of the zero-degree inelastic spectrum in the energy region where vibrational transitions are expected to occur. The possibility of a long-lived quartet CO^+ state³⁶ in our reactant-ion beam contributing to the smeared-out nature of the energy-loss spectrum was examined by lowering the ionizing electron energy to the approximate threshold for production of this electronically excited state. The position of peaks and shapes of inelastic energy-loss spectra at low electron energies were not observably different, within limits of error, from those measured at 60 eV and indicate that the reactant CO^+ ion beam is predominantly ($\geq 90\%$) in the $X^2\Sigma$ state.

Relative differential inelastic cross sections for 0° lab scattering are presented in Figs. 2–4 for different values of CO^+ kinetic energies. At high reactant-ion kinetic energies, correlation exists between peaks appearing in the inelastic spectra and arrows indicating vibrational excitation; however, there is an overlapping of peaks appearing in the spectra. A small amount of inelastic-peak broadening is expected from the finite velocity width of the incident-ion beam (shown as the solid curve in Fig. 2) and small out-of-plane Ar velocity components, but experimental widths of inelastic peaks are larger than expected for pure vibrational excitation, indicating simultaneous vibrational-rotational transitions. As reactant-ion kinetic energy is lowered, smaller inelastic energy losses predominate with evidence for collisional events below the threshold for the $\nu=0 \rightarrow 1$ vibrational transition corresponding to pure rotational excitation. Slight tailing of elastic peaks into the inelastic region result in larger errors for small energy losses, as shown in Fig. 4. This makes it difficult to ascertain the exact shape of the inelastic spectra

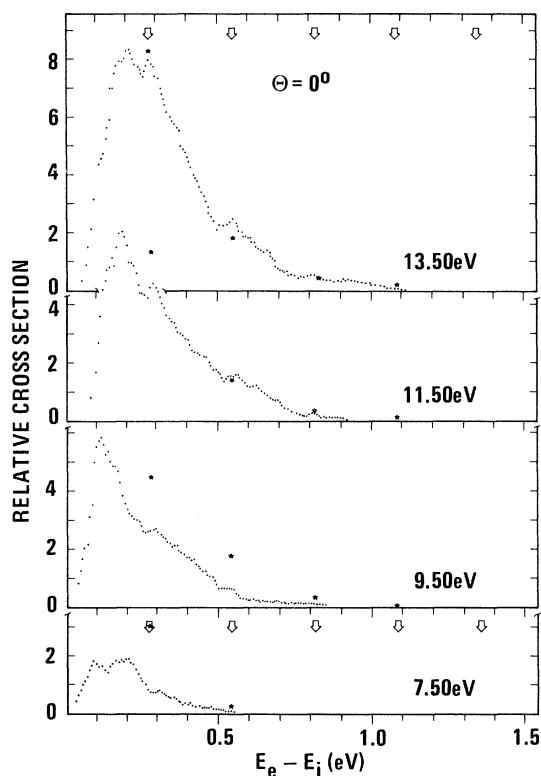


FIG. 3. Energy-loss spectra of CO^+ . Relative differential cross sections for inelastic CO^+ -Ar collisions vs inelasticity of collisions, $E_e - E_i$, at 0° lab scattering angle and several incident ion energies (E_0). The dots are experimental data. Arrows indicate calculated energy loss corresponding to vibrational $\nu=0 \rightarrow 1, \dots, 5$ excitation by collision, and stars indicate cross sections for each vibrational transition theoretically predicted by an oriented nonlinear encounter model, with calculated probabilities averaged over all molecular orientations.

below 0.125-eV energy loss, but the maxima observed below the $\nu=0 \rightarrow 1$ vibrational threshold occur at energies which require changes in rotational quantum number of approximately 20.

The decrease in vibrational transition probabilities with reactant-ion kinetic energies is similar to that observed in the oxygen system²⁵ where inelastic energy-loss data were in accord with a semi-classical forced-harmonic-oscillator model. Although exact quantum-mechanical calculations⁵ and exact classical treatments^{16,17} for certain systems exist, an attractive approach to the problem of translational vibrational energy conversion has been developed by Treanor⁹ using time-dependent wave-function solutions⁸ to the Schrödinger equation for a harmonic oscillator forced by a colliding atom. This solution to the time-dependent Schrödinger equation for the forced oscillator has been used to obtain an analytic expression⁹ for vibrational transition probabilities

$$P_{m,n} = m!n! e^{-\epsilon_0} \epsilon_0^{m+n} S_{m,n}^2, \quad (8)$$

where m is the stationary state at $t=0$ and n is the final state. $S_{m,n}$ is given by

$$S_{m,n} = \sum_{j=0}^u \frac{(-1)^j \epsilon_0^j}{(n-j)!j!(m-j)!}, \quad (9)$$

where u is the lesser of m and n . For $0 \rightarrow n$ transition, (9) reduces to

$$P_{0,n} = (1/n!) e^{-\epsilon_0} \epsilon_0^n. \quad (10)$$

ϵ_0 is the energy a classical oscillator would absorb if acted on by the forcing potential, divided by $\hbar\omega$:

$$\epsilon_0 = (2\mu\hbar\omega)^{-1} \left| \int_{-\infty}^{\infty} F(t) e^{i\omega t} dt \right|^2, \quad (11)$$

where ω is the frequency of the oscillator, μ is its reduced mass, and $F(t)$ is the force on the oscillator. Shin¹⁰ has formulated this same collision problem in terms of a time-independent Schrödinger equation and obtained Eq. (10) using a Green's-function method. $F(t)$ is derived from the intermolecular potential function which we have chosen

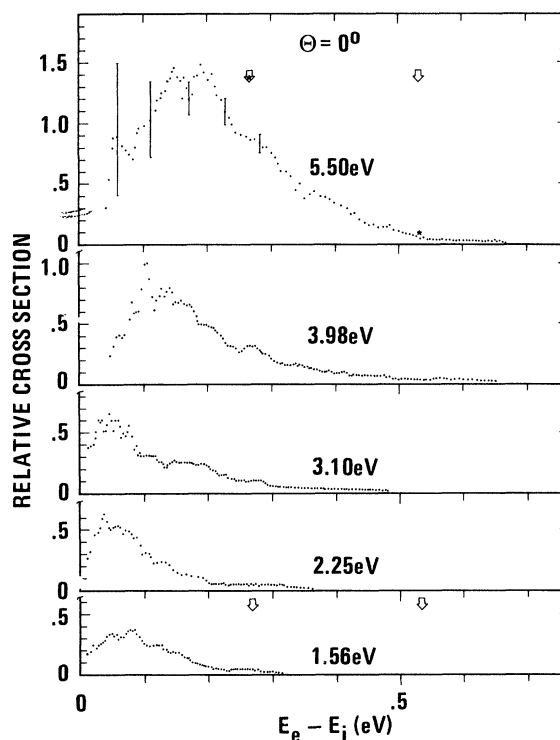


FIG. 4. Energy-loss spectra of CO^+ . Relative differential cross sections for inelastic CO^+ -Ar collisions vs inelasticity collisions, $E_e - E_i$, at 0° lab scattering angle and several incident ion energies (E_0). The dots are experimental data. Arrows indicate calculated energy loss corresponding to vibrational $\nu=0 \rightarrow 1, 2$ excitation by collision, and stars indicate cross sections for each vibrational transition theoretically predicted by an oriented nonlinear encounter model, with calculated probabilities averaged over all molecular orientations.

to be a Lennard-Jones potential between colliding atoms:

$$U(r_1, r_2) = 2D \sum_{i=1}^2 [(\sigma/r_i)^{12} - (\sigma/r_i)^6], \quad (12)$$

where

$$r_{1,2}^2 = r^2 \pm 2(d+x)rS_{2,1} \cos X + (d+x)^2 S_{2,1}^2. \quad (13)$$

$S_{1,2}$ is given by $m_{e,0}/(m_e + m_0)$, where the m 's refer to the masses of the respective atoms of the

diatomic. r is the distance between the atom and the center of mass of the molecules. The angle X between r and the bond axis of the molecule is assumed constant throughout the collision, d is the equilibrium internuclear distance in the molecule, x its vibrational amplitude, and D and σ are the Lennard-Jones (LJ) potential parameters. Neglecting terms in $(d+x)/r$ of third order or higher, Shin has shown that the potential can be expressed as a function of r , x , and X :

$$U(r, x, X) = 4D \left[\left(\frac{\sigma}{r} \right)^{12} - \left(\frac{\sigma}{r} \right)^6 \right] + 24D \left[\left(\frac{\sigma}{r} \right)^{12} - \frac{1}{2} \left(\frac{\sigma}{r} \right)^6 \right] (S_2 - S_1) \left(\frac{d+x}{r} \right) \cos X \\ + 4D \left[(42 \cos^2 X - 3) \left(\frac{\sigma}{r} \right)^{12} - 12 \cos^2 X - \frac{3}{2} \left(\frac{\sigma}{r} \right)^6 \right] (S_1^2 + S_2^2) \left(\frac{d+x}{r} \right)^2. \quad (14)$$

$F(t)$ computed from this potential is then used in Eq. (11) to evaluate ϵ_0 , with the dependence of r on time determined by the equation of motion

$$t = \left(\frac{1}{2} \tilde{m} \right)^{1/2} \int_{r^*}^r \frac{dr}{[E - E(b/r)^2 - U(r, x, X)]^{1/2}}, \quad (15)$$

where E is the initial relative kinetic energy, b is the impact parameter, and r^* is the largest root of the radical in the denominator. With $F(t)$ computed from $U(r)$ and t evaluated from Eq. (15), ϵ_0 determined from Eq. (11) has the form

$$\epsilon_0 = 2(\mu \hbar \omega)^{-1} \left[\left(\frac{2}{7} d \pi \tilde{m} \omega \right) (\cos^2 X - \frac{1}{14}) (S_1^2 + S_2^2) \right]^2 \left[1 - \frac{4 \cos^2 X - \frac{1}{2}}{14 \cos^2 X - 1} \left(\frac{1}{\Gamma(\frac{8}{7}) \gamma^{6/7}} \right) \right. \\ \left. + \left(\frac{14 D \gamma}{d \sigma \tilde{m} \omega^2} \right) \left(\frac{S_1 - S_2}{S_1^2 + S_2^2} \right) \left(\frac{\cos X}{\cos^2 X - \frac{1}{14}} \right) \left(1 - \frac{2 \gamma^{6/7}}{\Gamma(\frac{13}{7})} \right) \right]^2 e^{-2\omega t}, \quad (16)$$

where

$$\gamma = \left(\frac{1}{14} \omega a \right) (\tilde{m}/2D)^{1/2},$$

$$a = \frac{\sigma}{\pi^{1/2}} \frac{\Gamma(\frac{7}{12})}{\Gamma(\frac{1}{12})} \left(\frac{4D}{E} \right)^{1/12} \left[1 - \frac{1}{72} \left(\frac{\Gamma(\frac{1}{12})}{\Gamma(\frac{7}{12})} \right)^2 \left(\frac{D}{E} \right)^{1/2} \right] \left[1 - \frac{2}{\pi} \left(\frac{D}{E} \right)^{1/2} \right]^{-1}, \\ r = \left[\frac{\Gamma(\frac{7}{12})}{\Gamma(\frac{1}{12})} \left(\frac{\pi \tilde{m}}{2} \right)^{1/2} \frac{(4D \rho_1)^{1/2} \sigma}{E^{7/12}} \right] \left[1 - \frac{1}{72} \left(\frac{\Gamma(\frac{1}{12})}{\Gamma(\frac{7}{12})} \right)^2 \left(\frac{D}{E} \right)^{1/2} \frac{\rho_2}{\rho_1^{1/2}} \right] + \frac{5}{144} \frac{\Gamma(\frac{5}{12})}{\Gamma(\frac{1}{12})} \left(\frac{\pi \tilde{m}}{2} \right)^{1/2} \left(\frac{b^2}{(\sigma(4D))^{1/12} \rho_1^{1/6} E^{5/12}} \right), \quad (17)$$

$$\rho_1 = 1 + (S_1^2 + S_2^2)(42 \cos^2 X - 3)(d/r^*)^2 + 6(S_2 - S_1) d/r^* \cos X,$$

$$\rho_2 = 1 + (S_1^2 + S_2^2)(12 \cos^2 X - \frac{3}{2})(d/r^*)^2 + 3(S_2 - S_1) d/r^* \cos X.$$

Using this model developed by Shin we have computed vibrational transition probabilities with Eqs. (8) and (16) using a reduced impact parameter $b^* = b/\sigma$ as a variable to fit the inelastic energy-loss spectra in Figs. 2-4.

LJ parameters⁵³ $D = 1.612 \times 10^{-14}$ erg and $\sigma = 3.504$ Å were used along with the CO⁺ spectroscopic constants⁵² $\omega_e = 2214.24$ cm⁻¹, $\omega_e x_e = 15.16$ cm⁻¹, and $d = 1.1150$ Å. Since molecules in these ion-impact experiments will be randomly oriented, $U(r, X)$ and $P_{m,n}$ are calculated for many X to give

excitation probabilities which are then averaged over all molecular orientations. The relative differential cross sections are related to probabilities for inelastic scattering events at given impact parameters through the equation⁵⁴

$$\frac{\bar{I}_1}{\bar{I}_2} = \frac{P_1 b_1^* / \sin \phi_1}{P_2 b_2^* / \sin \phi_2} \frac{[db^*/d\phi]_1}{[db^*/d\phi]_2}, \quad (18)$$

in which ϕ is the center-of-mass scattering angle. Standard relations⁵⁵ have been used to relate ϕ to the inelastic energy-loss data measured at a given

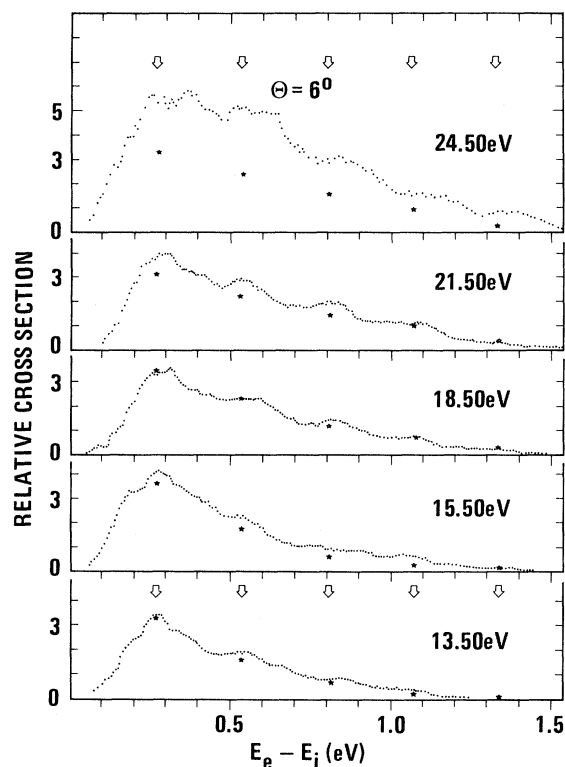


FIG. 5. Energy-loss spectra of CO^+ . Relative differential cross sections for inelastic $\text{CO}^+\text{-Ar}$ collisions vs inelasticity of collisions, $E_e - E_i$, at 6° lab scattering angle and several incident ion energies (E_0). The dots are experimental data. Arrows indicate calculated energy loss corresponding to vibrational $\nu=0 \rightarrow 1, \dots, 5$ excitation by collision, and stars indicate cross sections for each vibrational transition theoretically predicted by an oriented nonlinear encounter model, with calculated probabilities averaged over all molecular orientations.

lab angle Θ . With finite angular resolution, it is possible for inelastic processes appearing at 0° lab scattering angle to occur over a range of impact parameters and we have thus integrated the expression $P(b^*) b^* db^*$ from a minimum impact parameter b_{\min}^* to infinity for comparison with the experimental data. We have taken the relative $\nu=0 \rightarrow 1$ vibrational cross section at 0° and 15.50 eV energy as the point of normalization with which to compare the semiclassical model with our experimental data. The stars in Figs. 2-4 represent the relative cross sections computed from this treatment. As shown in Figs. 2-4 there is reasonable agreement between experimental and computed cross sections represented by small stars. It is to be remembered that b^* has been taken as a variable parameter with which to compare the predictions of theory and experiment. We have chosen values of b_{\min}^* that predict the magnitude of the cross sections and relative importance of

$\nu=0 \rightarrow 1, 2, 3$ vibrational cross sections at a given reactant-ion kinetic energy. Comparisons between experiment and the predictions of the model were not attempted below 5.50 eV energy in Fig. 4, since inelastic energy losses smaller than those for vibrational transitions predominate, as is typical of rotational excitation.

Additional comparisons between the forced oscillator model and experiment are given in Figs. 5 and 6 for 6° lab scattering angle. Reduced impact parameters used to calculate $P_{m,n}$ (averaged over all X) are presented in Table I for different values of E_0 .

As shown in Figs. 5 and 6, experimental data support the use of this theoretical model in inelastic events at small scattering angles. Fig. 7 presents similar data taken at 10° lab angle but here the comparison of theory and experiment is disconcerting in two respects. First, numerical

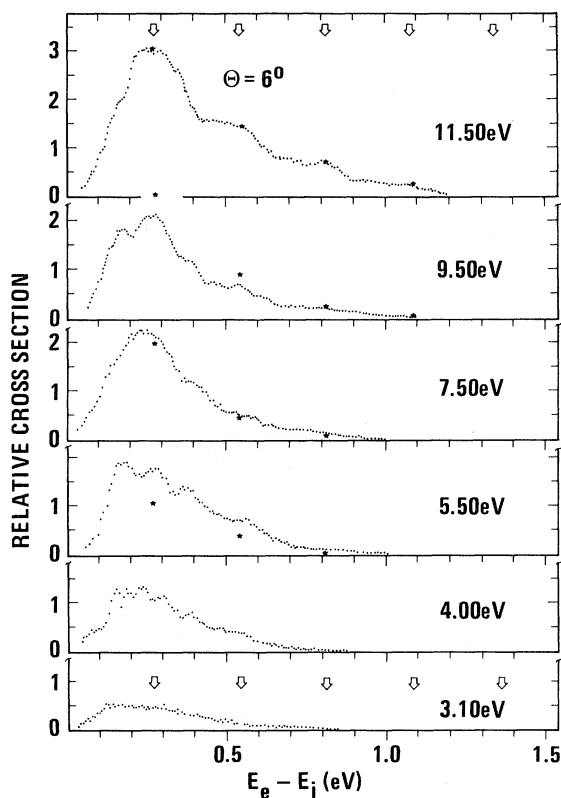


FIG. 6. Energy-loss spectra of CO^+ . Relative differential cross sections for inelastic $\text{CO}^+\text{-Ar}$ collisions vs inelasticity of collisions, $E_e - E_i$, at 6° lab scattering angle and several incident ion energies (E_0). The dots are experimental data. Arrows indicate calculated energy loss corresponding to vibrational $\nu=0 \rightarrow 1, \dots, 5$ excitation by collision, and stars indicate cross sections for each vibrational transition theoretically predicted by an oriented nonlinear encounter model, with calculated probabilities averaged over all molecular orientations.

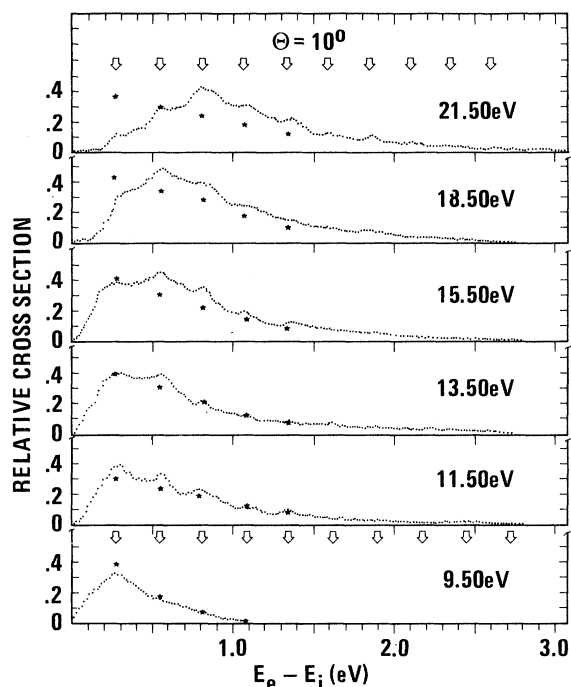


FIG. 7. Energy-loss spectra of CO^+ . Relative differential cross sections for inelastic CO^+ -Ar collisions vs inelasticity of collisions, $E_e - E_i$, at 10° lab scattering angle and several incident ion energies (E_0). The dots are experimental data. Arrows indicate calculated energy loss corresponding to vibrational $\nu = 0 \rightarrow 1, \dots, 10$ excitation by collision, and stars indicate cross sections for each vibrational transition theoretically predicted by an oriented nonlinear encounter model, with calculated probabilities averaged over all molecular orientations.

values of computed cross sections, presented as stars in Fig. 7, have been multiplied by 0.25 in order to place them on the same scale as experimental data. Second, the theory predicts $\nu = 0 \rightarrow 1$ to be the most likely transition, whereas multi-quantum transitions are experimentally observed to predominate at higher energies. In this 10° , 15.50 eV spectrum the model breaks down, as

TABLE I. Reduced impact parameter b^* used in X -averaged Shin model for comparison with experimental data.

Lab energy E_0 (eV)	Lab angle	
	0° b_{min}^*	6° b^*
24.5	1.19	1.13
21.5	1.13	1.08
18.5	1.07	1.04
15.5	1.01	0.98
13.5	0.97	0.93
11.5	0.92	0.86
9.5	0.87	0.79
7.5	0.80	0.70
5.5	0.70	0.60

applied to the present work, because it is at this energy and angle that multi-quantum transitions are observed to have higher relative cross section than $\nu = 0 \rightarrow 1$ transitions. The values of b^* that give the most reasonable fit (shown as stars) to the experimental data in Fig. 7 at each energy are 0.08 \AA smaller than the b^* 's given in Table I for $\Theta = 6^\circ$. Since molecules are expected to have a random initial distribution in X , cross sections have been computed from X averaged vibrational transition probabilities using the Shin oriented nonlinear collision model in which X is taken constant during individual collisions. However, it is possible that the assumption of taking X to be constant is not correct and considering X independent of ν may not adequately describe the detailed dynamics of the encounter, although ion-molecule interaction times are shorter than characteristic rotational times. The variation of $P_{m,n}$ with $m - n = 1, \dots, 5$ with X is shown in Fig. 8 for the $\text{CO}^+ X^2\Sigma + \text{Ar}$ system, where probabilities are given as a function of X for several values of b^* at $E_0 = 21.50$ eV. Solid curves representing transition probabilities are plotted for different initial orientation angles X . For large impact parameters, respective probabilities vary slowly with X , but a rapid variation of vibrational transitions with angle occurs for

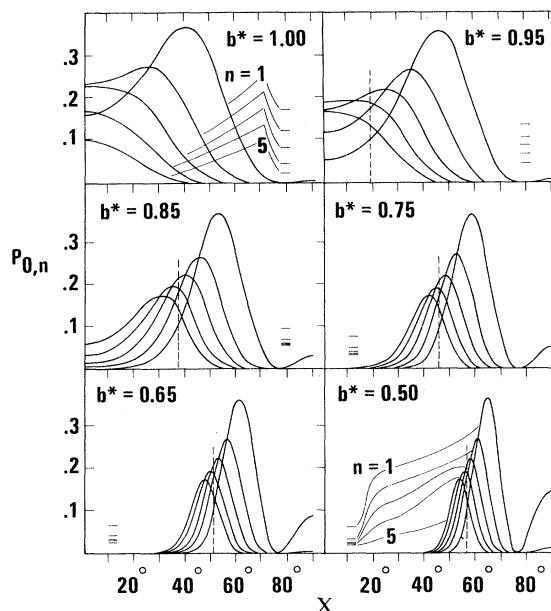


FIG. 8. Preferred orientation for vibrational excitation for 21.50-eV collision induced transition, $P_{0,n}$, for vibrational transitions $\nu = 0 \rightarrow n$, $n = 1, \dots, 5$ vs molecular orientation in collision X calculated from Eq. (16) for several reduced impact parameters b^* . The horizontal lines show corresponding values for $P_{0,n}$ averaged over all X . The dashed vertical line indicates the preferred molecular orientation which gives probabilities in agreement with observed cross sections at 10° and 21.50 eV.

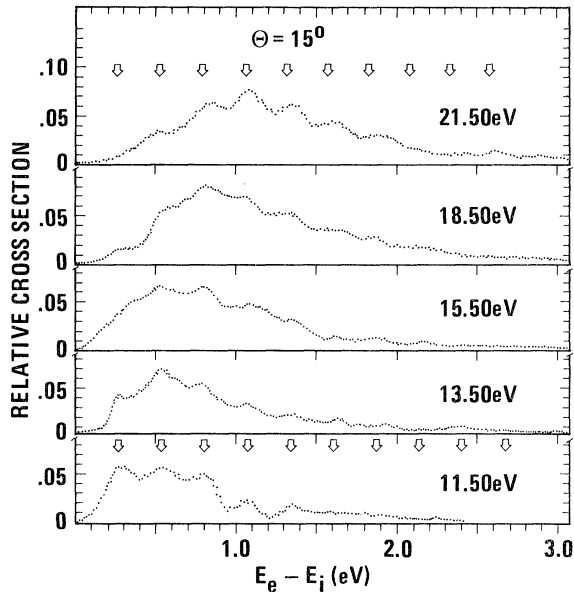


FIG. 9. Energy-loss spectra of CO^+ . Relative differential cross sections for inelastic CO^+ -Ar collisions vs inelasticity of collisions, $E_e - E_i$, at 15° lab scattering angle and several incident ion energies (E_0). The dots are experimental data. Arrows indicate calculated energy loss corresponding to vibrational $\nu=0 \rightarrow 1, \dots, 10$ excitation by collision.

small b^* . Small horizontal lines in each diagram of this figure display angle-averaged probabilities. It is noticed that computed P_{0-1} 's dominate angle-averaged transition probabilities, a fact inconsistent with the inelastic energy loss presented in Fig. 7. The dashed vertical lines in this figure indicate molecular orientations for various values of b^* that give probabilities in agreement with the cross section measured at $E_0 = 21.50$ eV and 10° lab scattering angle. For example, CO^+ colliding with Ar at 21.50 eV, $b^* = 0.85$ and $X = 37^\circ$, would have the transition probability greatest for $\nu = 0 \rightarrow 3$ and least for $\nu = 0 \rightarrow 1$.

Inelastic energy losses for $\Theta = 10^\circ$ and 20° lab scattering angles presented in Figs. 9 and 10 clearly show the predominance of multiquantum jump transitions. As shown here, multiquantum vibrational processes increase with lab scattering angle and energy. Maxima in these spectra appear at energies approximating those calculated using Eq. (3) for pure vibrational excitations. Comparison of data in Figs. 9 and 10 with the forced oscillator model is not shown since computed cross section can neither be placed on scale or fitted with b^* to give transitions probabilities approximating observation and a question arises regarding the applicability of the interaction potential taken for the $\text{CO}^+X^2 + \text{Ar}$ system. $U(r)$ in Eq. 12 does not consider the r^{-4} polarization terms. While inclusion of r^{-4} terms would signif-

TABLE II. Values of reduced impact parameter b^* that result in equivalent X -averaged vibrational probabilities for different interaction potential parameters.

$D = 1.612 \times 10^{-14}$ erg $\sigma = 3.504 \text{ \AA}$	$D = 1.612 \times 10^{-14}$ erg $\sigma = 2.95 \text{ \AA}$	$D = 2.0 \times 10^{-14}$ erg $\sigma = 2.90 \text{ \AA}$
$b^* = 0.50$	$b^* = 0.70$	$b^* = 0.70$
0.55	0.75	0.75
0.60	0.80	0.80
0.65	0.85	0.85
0.70	0.90	0.90
0.75	0.95	0.95
0.80	1.00	1.00
0.85	1.03	1.05
0.90	1.06	1.10
0.95	1.10	1.15
1.00	1.15	1.20
1.05	1.20	1.25
1.10	1.25	1.30

icantly alter the shape of the potential in regions of the minimum, the effect is less pronounced in strongly repulsive portions with a relatively small effect⁵⁶ on the computed transition probabilities. Jordan *et al.*⁵⁷ have used high-energy scattering of neutral particles to obtain an empirical potential for the neutral CO -Ar system. They find $U(r)$ is given by $551/r^{6.99}$ eV for $2.09 < r < 2.68$, which should approximate that for the ionic system studied in this work. $U(r_1, r_2)$ from Eq. (12) using the LJ parameters is considerably higher at $r = 2.4 \text{ \AA}$ than the experimentally determined potential. We have fitted the potential from Eq. (12) at $r = 2.43 \text{ \AA}$ to the potential of Jordan *et al.*⁵⁷ by a proper choice of D and σ in order to investigate the effect of b^* of such a fitted potential. The results are shown in Table II where the b^*

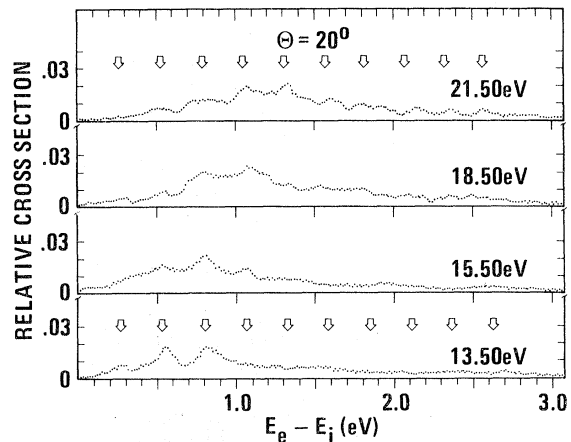


FIG. 10. Energy-loss spectra of CO^+ . Relative differential cross sections for inelastic CO^+ -Ar collisions vs inelasticity of collisions, $E_e - E_i$, at 20° lab scattering angle and several incident ion energies (E_0). The dots are experimental data. Arrows indicate calculated energy loss corresponding to vibrational $\nu=0 \rightarrow 1, \dots, 10$ excitation by collision.

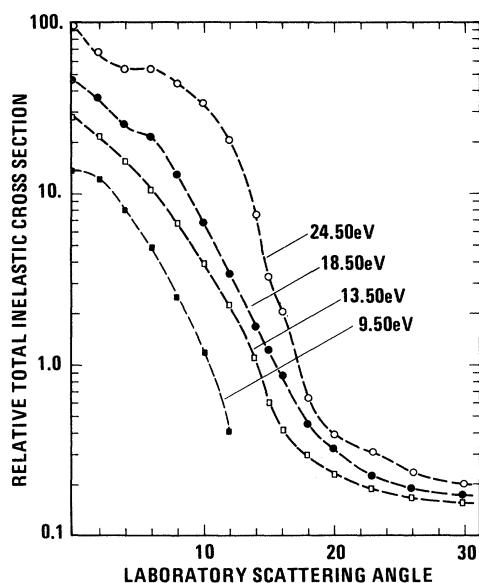


FIG. 11. Relative total inelastic cross section for inelastic scattering of CO^+ by Ar vs lab scattering angle for several incident-ion kinetic energies.

on each line results in similar predicted vibrational excitation probabilities for given values of E_0 . It is seen that an equally adequate fit to the experimental spectra can be achieved with slightly different values of b^* in the theoretical description. The modified b^* 's in the second and third columns of Table II are obtained with LJ parameters fitted to

the experimental potential, but there is an indeterminacy in the fitted potential since a small variation in σ can be compensated by a change in D when computing b^* . The applicability of the Shin model to vibrational excitations occurring at large impact parameters is, however, demonstrated in Figs. 2-7, where measured and computed cross sections are in agreement. Although this model does not adequately describe inelastic scattering for lab angles larger than 10° , the predominant scattering processes occur at smaller angles with small energy losses where the model is applicable. The dependence of total CO^+ -Ar cross sections on angle are shown in Fig. 11, where the majority of inelastic events are observed to produce products scattered at small angles.

In summary, the cross sections for vibrational excitations in CO^+ -Ar collisions have been obtained from inelastic energy-loss measurements and are found to compare reasonably well with a semiclassical impact parameter model at small scattering angles. Disagreement between theory and experiment is noted at larger scattering angles, where multiquantum transitions predominate in contrast to the predictions of the semiclassical model. Inelasticities in the collision events increase with ion kinetic energy and scattering angle, although cross sections are largest for small angle scattering. The widths of peaks in the inelastic spectrum indicate simultaneous vibrational-rotational excitations with pure rotational transitions dominant at low reactant-ion kinetic energy.

*Research supported by National Aeronautics and Space Administration under Grant No. NSG-657.

¹K. Takayanagi, *Advan. At. Mol. Phys.* **1**, 149 (1965); *Progr. Theoret. Phys. (Kyoto) Suppl.* **25**, 1 (1963).

²D. Rapp and T. Kassal, *Chem. Rev.* **69**, 61 (1969).

³K. F. Herzfeld and T. A. Litovitz, *Adsorption and Dispersion of Ultrasonic Waves* (Academic, New York, 1959), Chap. VII.

⁴T. L. Cottrell and J. C. McCoubrey, *Molecular Energy Transfer in Gases* (Butterworths, London, 1961).

⁵M. Salkoff and E. Bauer, *J. Chem. Phys.* **29**, 26 (1958).

⁶F. H. Mies and K. E. Shuler, *J. Chem. Phys.* **37**, 177 (1962).

⁷R. Marriott, *Proc. Phys. Soc. (London)* **84**, 877 (1964).

⁸E. H. Kerner, *Can. J. Phys.* **36**, 371 (1958).

⁹C. E. Treanor, *J. Chem. Phys.* **43**, 532 (1965); **44**, 2220 (1966).

¹⁰H. K. Shin, *J. Phys. Chem.* **73**, 4321 (1969); *Chem. Phys. Letters* **5**, 137 (1970); **7**, 436 (1970); *J. Chem. Phys.* **49**, 3964 (1968).

¹¹D. A. Micha and M. Rotenberg, *Chem. Phys. Letters* **6**, 79 (1970).

¹²C. F. Hansen and W. E. Pearson, *J. Chem. Phys.* **53**, 3557 (1970).

¹³V. P. Gutschick, V. McKoy, and D. J. Diestler, *J. Chem. Phys.* **52**, 4807 (1970).

¹⁴S. W. Benson, G. C. Berend, and J. C. Wu, *J. Chem. Phys.* **37**, 1386 (1962).

¹⁵D. Secrest and B. R. Johnson, *J. Chem. Phys.* **45**, 4556 (1966).

¹⁶J. D. Kelley and M. Wolfsberg, *J. Chem. Phys.* **53**, 2967 (1970); **44**, 324 (1966); J. D. Kelley, *ibid.* **53**, 3864 (1970).

¹⁷D. J. Wilson, *J. Chem. Phys.* **54**, 540 (1971); D. J. Locker and D. J. Wilson, *ibid.* **52**, 271 (1970); R. Dubrow and D. J. Wilson, *ibid.* **50**, 1553 (1969).

¹⁸R. G. Gordon, W. Klemperer, and J. T. Steinfeld, *Ann. Rev. Phys. Chem.* **19**, 215 (1968).

¹⁹C. Ottinger, R. Velasco, and R. N. Zare, *J. Chem. Phys.* **52**, 1636 (1970).

²⁰D. L. Akins, E. H. Fink, and C. B. Moore, *J. Chem. Phys.* **52**, 1604 (1970), and also C. B. Moore, *Accts. Chem. Res.* **2**, 103 (1969).

²¹J. Schöttler and J. P. Toennies, *Z. Physik* **214**, 472 (1968); W. D. Held, J. Schöttler, and J. P. Toennies, *Chem. Phys. Letters* **6**, 304 (1970).

²²P. F. Dittner and S. Datz, *J. Chem. Phys.* **49**, 1969 (1968).

²³J. H. Moore and J. P. Doering, *Phys. Rev. Letters* **23**, 564 (1969); *J. Chem. Phys.* **52**, 1692 (1970).

²⁴M. H. Cheng, M. H. Chiang, E. A. Gislason, B. H. Mahan, C. W. Tsao, and A. S. Werner, *J. Chem. Phys.* **52**, 6150 (1970).

- ²⁵T. F. Moran and P. C. Cosby, *J. Chem. Phys.* **51**, 5724 (1969); P. C. Cosby and T. F. Moran, *ibid.* **52**, 6157 (1970).
- ²⁶T. F. Moran, F. Petty, and G. S. Turner, *Chem. Phys. Letters* **9**, 379 (1971).
- ²⁷D. Beck and H. Förster, *Z. Physik* **240**, 136 (1970).
- ²⁸W. Paul and H. Steinwedel, *Z. Naturforsch* **8a**, 448 (1953); W. Paul, H. P. Reinhard, and U. von Zahn, *Z. Physik* **152**, 143 (1958); R. F. Post, University of California Radiation Laboratory Report No. UCRL-2209, 1953 (unpublished).
- ²⁹R. N. Fox, R. L. Fitzwilson, and E. W. Thomas, *J. Phys. E* **3**, 36 (1970); E. Yellin, L. I. Yin, and I. Adler, *Rev. Sci. Instr.* **41**, 18 (1970).
- ³⁰P. Marmet and L. Kerwin, *Can. J. Phys.* **38**, 787 (1960); G. J. Schulz, *Phys. Rev.* **125**, 299 (1962).
- ³¹J. J. Leventhal and G. R. North, *Rev. Sci. Instr.* **42**, 120 (1971); H. Wollnik, in *Focusing of Charged Particles*, edited by A. Septier (Academic, New York, 1967), Vol. II, p. 163; A. L. Hughes and J. H. McMillen, *Phys. Rev.* **34**, 291 (1929).
- ³²R. H. Jones, D. R. Olander, and V. R. Kruger, *J. Appl. Phys.* **40**, 4641 (1969); **40**, 4650 (1969); **41**, 2769 (1970); **41**, 4388 (1970); **41**, 4392 (1970).
- ³³J. T. Park, F. D. Schowengerdt, and D. R. Schoonover, *Phys. Rev. A* **3**, 679 (1971); D. R. Schoonover and J. T. Park, *ibid.* **3**, 228 (1971); J. T. Park, D. R. Schoonover, and G. W. York, *ibid.* **2**, 2304 (1970).
- ³⁴J. Baudon, M. Barat, and M. Abignoli, *J. Phys. B* **1**, 1083 (1969); **3**, 207 (1970); M. Baudon, J. Barat, M. Abignoli, and J. C. Houver, *ibid.* **3**, 230 (1970).
- ³⁵W. Aberth and D. C. Lorents, *Phys. Rev.* **182**, 162 (1969); D. Coffery, Jr., D. C. Lorents, and F. T. Smith, *ibid.* **187**, 201 (1969).
- ³⁶T. F. Moran, F. C. Petty, and A. F. Hedrick, *J. Chem. Phys.* **51**, 2112 (1969).
- ³⁷J. F. M. Aarts and F. J. De Heer, *Physica* **49**, 425 (1970).
- ³⁸D. C. Jain and R. C. Sahni, *Intern. J. Quantum Chem.* **2**, 325 (1968).
- ³⁹T. F. Moran and L. Friedman, *J. Chem. Phys.* **42**, 2391 (1965).
- ⁴⁰J. Desesquelles, M. Dufay, and M. C. Poulizac, *Phys. Letters* **27A**, 96 (1968).
- ⁴¹J. Hesser, *J. Chem. Phys.* **48**, 2518 (1968).
- ⁴²E. H. Fink and K. H. Welge, *Z. Naturforsch.* **23a**, 358 (1968).
- ⁴³G. M. Lawrence, *J. Quant. Spectry. Radiative Transfer* **5**, 359 (1965).
- ⁴⁴R. G. Bennett and F. W. Dalby, *J. Chem. Phys.* **31**, 434 (1959).
- ⁴⁵R. W. Nicholls, *Can. J. Phys.* **40**, 1772 (1962).
- ⁴⁶P. H. Krupenie, *Natl. Std. Ref. Data Ser.*, *Natl. Bur. Std. (U. S.) NSRDS-NBS 5* (1966).
- ⁴⁷D. C. Lorents and W. Aberth, *Phys. Rev.* **139**, A1017 (1965).
- ⁴⁸R. L. Champion, L. D. Doverspike, W. G. Rich, and S. M. Bobbio, *Phys. Rev. A* **2**, 2327 (1970).
- ⁴⁹K. W. Ford and J. A. Wheeler, *Ann. Phys. (N.Y.)* **7**, 259, 287 (1959).
- ⁵⁰R. B. Bernstein, *Advan. Chem. Phys.* **10**, 75 (1966).
- ⁵¹J. C. Y. Chen, C. Wang, and K. M. Watson, *Phys. Rev. A* **1**, 1150 (1970).
- ⁵²G. Herzberg, *Molecular Spectra and Molecular Structure I. Spectra of Diatomic Molecules* (Van Nostrand, Princeton, N.J., 1967).
- ⁵³J. O. Hirschfelder, C. F. Curtiss, and R. B. Bird, *Molecular Theory of Gases and Liquids* (Wiley, New York, 1964).
- ⁵⁴R. D. Levine and R. B. Berstein, *Israel J. Chem.* **7**, 315 (1969).
- ⁵⁵L. I. Schiff, *Quantum Mechanics* (McGraw-Hill, New York, 1968), p. 111.
- ⁵⁶H. K. Shin, *Chem. Phys. Letters* **5**, 137 (1970).
- ⁵⁷J. E. Jordon, S. O. Colgate, I. Amdur, and E. A. Mason, *J. Chem. Phys.* **52**, 1143 (1970).

Rotational-Vibrational Excitation of H₂ by Slow Electrons*

Ronald J. W. Henry

*Department of Physics and Astronomy, Louisiana State University,
Baton Rouge, Louisiana 70803*

and

Edward S. Chang

*Department of Physics and Astronomy, University of Massachusetts,
Amherst, Massachusetts 01002*

(Received 2 June 1971)

The frame-transformation theory is applied to a calculation of electron scattering from H₂ in the energy range of 1–10 eV. Results are presented for differential as well as integrated cross sections for pure vibrational and rotational-vibrational excitation processes. Our calculations are in very satisfactory agreement with experiment and are subject to easy interpretation.

I. INTRODUCTION

The theory of frame transformation and its application to electron-molecule scattering have been

discussed by Chang and Fano¹ (CF). In this paper, we adapt it to calculate rotational-vibrational cross sections in H₂ by electron impact, in the energy range 1–10 eV. We choose H₂ as the target mole-